High energy electron fluxes in dc-augmented capacitively coupled plasmas I. Fundamental characteristics

Mingmei Wang[1,a)] and Mark J. Kushner[2,b)]
[1]*Department of Chemical and Biological Engineering, Iowa State University, Ames, Iowa 50010, USA*
[2]*Department of Electrical Engineering and Computer Science, University of Michigan, 1301 Beal Ave., Ann Arbor, Michigan 48109, USA*

(Received 14 September 2009; accepted 7 December 2009; published online 29 January 2010)

Power deposition from electrons in capacitively coupled plasmas (CCPs) has components from stochastic heating, Joule heating, and from the acceleration of secondary electrons through sheaths produced by ion, electron, or photon bombardment of electrodes. The sheath accelerated electrons can produce high energy beams which, in addition to producing excitation and ionization in the gas can penetrate through the plasma and be incident on the opposite electrode. In the use of CCPs for microelectronics fabrication, there may be an advantage to having these high energy electrons interact with the wafer. To control the energy and increase the flux of the high energy electrons, a dc bias can be externally imposed on the electrode opposite the wafer, thereby producing a dc-augmented CCP (dc-CCP). In this paper, the characteristics of dc-CCPs will be discussed using results from a computational study. We found that for a given rf bias power, beams of high energy electrons having a narrow angular spread ($<1°$) can be produced incident on the wafer. The maximum energy in the high energy electron flux scales as $\varepsilon_{max}=-V_{dc}+V_{rf}+V_{rf0}$, for a voltage on the dc electrode of V_{dc}, rf voltage of V_{rf}, and dc bias on the rf electrode of V_{rf0}. The dc current from the biased electrode must return to ground through surfaces other than the rf electrode and so seeks out a ground plane, typically the side walls. If the side wall is coated with a poorly conducting polymer, the surface will charge to drive the dc current through. © *2010 American Institute of Physics*. [doi:10.1063/1.3290870]

I. INTRODUCTION

The successful use of radio frequency (rf) capacitively coupled plasmas (CCPs) in microelectronics fabrication is predicated on being able to control the energy and angular distributions of reactant species to the wafer.[1] In conventional, single frequency CCPs, there is a tradeoff between controlling the ion energy and angular distribution (IEAD) and the rate of plasma production as a function of excitation frequency and gas pressure.[2] More advanced two-frequency CCPs separate these functions by attempting to control the IEAD using low frequency (LF) excitation (<tens of megahertz) and using a high frequency (HF) excitation (>tens of megahertz) to control the production of the plasma and so the magnitude of fluxes to the substrate.[3]

New designs of CCPs are intended to provide additional control of the reactant fluxes to the substrate. One such example is a dc-augmented CCP (dc-CCP).[4–7] In this design, the electrode opposite the wafer is biased with a dc voltage (V_{dc}) with the intent of producing a high energy electron (HEE) beam onto the wafer having a narrow angular distribution. The HEE is thought to have beneficial effects in controlling the profile of high aspect ratio features during plasma etching. Since the dc biases for dc-CCPs operating at tens of millitorr are typically many hundreds of volts, ion acceleration into the dc electrode, typically made of Si, can also sputter Si atoms into the plasma. As such, the dc-CCP can also provide some additional control over reaction chemistry.

Etching of high aspect ratio features for microelectronics fabrication is challenged to obtain reproducible features with straight walls and definable shapes. For example, holes with diameters of tens of nanometers with high aspect ratios (HARs) in excess of 70 are being fabricated in large arrays for memory cells.[8] One of the challenging aspects of these processes is the errant and nearly random occurrence of features that twist.[8–10] That is, instead of etching vertically, the feature will turn to the side, often after a significant fraction of the feature has already been etched. The direction of twisting, its frequency of occurrence, and its proximity to other twisting features typically has no discernable pattern.

One possible explanation for twisting is errant charging and dc-CCPs have been proposed as a remedy.[5,7] As the feature size shrinks to have an opening area of only hundreds of nm^2 the rate of entry of radicals and ions into the feature begins to become statistical. For example, the time between the arrivals of two ions into a feature 50 nm in diameter for a flux of 10^{16} cm^{-2} s^{-1} is 5 μs. This small rate of particle arrival leads to feature-to-feature statistical variations in the neutral and charged fluxes entering a single feature. Ions arriving onto the wafer after acceleration through the sheath have a narrower angular distribution than do thermal electrons. The end result is that ions penetrate deeper into features, producing random charging and electric fields that may deflect subsequent ions and produce twisting. The HEE flux

a)Electronic mail: mmwang@iastate.edu.
b)Author to whom correspondence should be addressed. Electronic mail: mjkush@umich.edu.

 © 2010 American Institute of Physics

Author complimentary copy. Redistribution subject to AIP license or copyright, see http://jap.aip.org/jap/copyright.jsp

with its narrow angular distribution may be able to penetrate into HAR features and possibly neutralize this errant positive charge.

Both experiments and simulations have been conducted to investigate the characteristics of HEEs in dc-CCPs. Kawamura *et al.*[4] analytically analyzed dc-CCPs, and found that a *dc/rf sheath* develops on the negatively biased electrode, while an rf sheath develops on the opposite electrode. The voltage drop in the rf sheath is nearly independent of the dc voltage if the rf power is held constant. Recently, they also conducted detailed analysis of secondary electron trapping and investigated the energy distributions of secondary electron fluxes incident onto the substrate.[5] Particle-in-cell simulations of dc-CCPs were performed having a dc and a 4 MHz bias on the top electrode, while the bottom electrode was grounded. Their simulations showed good agreement with the analytic solutions. They found that adding V_{dc} to the rf electrode increases the mean secondary electron energy, which results in a higher discharge efficiency. Adding V_{dc} altered the fraction of the rf cycle during which secondary electrons emitted from electrodes were trapped so that more secondary electrons impinge on the wafer with higher energy.

Denpoh *et al.*[6] examined the role of HEEs in a dc-CCP using a one-dimensional test particle Monte Carlo simulation. In their work, a dc bias was applied on the top electrode and an rf bias at 2 MHz was applied on the bottom electrode. They found that when the rf source was off and dc source was on, HEEs reached the wafer but they did not have a large influence on discharge efficiency due to their lack of confinement. When both the rf source and dc source were on, the HEEs were thermalized due to the confinement from a time averaged potential well produced by the rf bias.

The properties of HEEs were also measured experimentally by Xu *et al.*[7] using a single frequency dc-CCP with a dc bias applied on the top electrode and a rf bias at 13.56 MHz applied to the bottom electrode. They proposed that the rf cycle was divided to two regimes: a dumping regime and a trapping regime. The trapping regime is when the rf sheath potential is highly negative. HEEs are thermalized and returned to the bulk plasma, which contributes to a higher discharge efficiency. In the dumping regime, the rf sheath potential is positive. HEEs are accelerated by the rf sheath and penetrate it to reach the substrate. These highly energetic and directional electrons were anticipated to neutralize positive charges deep in features. At $V_{dc}=-800$ V, the HEE current was comparable to the ion current.

In this paper, the properties of HEE beams produced in dc-CCPs sustained in Ar will be discussed with results from a two-dimensional computational investigation. In our companion paper these properties will be used to investigate the means to remedy twisting during HAR etching in SiO_2 in dc-CCPs sustained in $Ar/C_4F_8/O_2$ gas mixtures.[11] We found that for a given rf bias power, beams of HEEs having narrow angular spread ($<1°$) can be produced incident on the wafer resulting from secondary electron emission from the dc biased electrode. The maximum energy in the HEE flux scales $\varepsilon_{max}=-V_{dc}+V_{rf}+V_{rf0}$ for a voltage on the dc electrode of V_{dc}, rf voltage on the lower electrode of V_{rf}, and dc bias on the rf electrode of V_{rf0}. Depending on the phase and amplitude of the rf voltage, secondary electrons from the dc electrode may be trapped in the plasma. Similarly, HEEs resulting from secondary electrons emitted from the rf biased electrode can reflect from the dc electrode and be incident onto the wafer. The dc current from the biased electrode must return to ground through surfaces other than the capacitively coupled rf electrode and so seeks out a ground plane. For our geometry, the ground plane is the side walls of the reactor. If a poorly conducting polymer is deposited on the side wall, the polymer surface will charge to drive the required dc current through the polymer layer.

The model used in this investigation is described in Sec. II followed by our discussion of properties of dc-CCPs sustained in argon in Sec. III. Our concluding remarks are in Sec. IV.

II. DESCRIPTION OF THE MODEL

The two-dimensional hybrid plasma equipment model (HPEM) was used in this investigation. The HPEM has been previously discussed in detail,[12] and so is only briefly described here. The HPEM is a two-dimensional model which consists of separate modules which address different physical phenomena. Each module consists of a time integration over many rf cycles, during which plasma quantities (e.g., densities and temperatures) are either recorded as a function of position and phase or recorded only as position dependent quantities averaged over the rf cycle. These values are then passed to the next module and the process iterated to a cycle-average steady state. The modules used in this study are the (1) Electron Monte Carlo Simulation (EMCS) for sheath accelerated secondary electrons, (2) the Fluid Kinetics Module (FKM) to obtain densities, fluxes, and energies of all charged and neutral species, as well as the electric potential from the solution of Poisson's equation, and (3) the Plasma Chemistry Monte Carlo Module to obtain the energy and angular distributions of neutrals and charged species striking the wafer.

In the FKM, continuity, momentum, and energy equations are separately solved for all nonelectron species (neutrals and ions). Coupling between these fluids is through collisional exchange for momentum and energy. For bulk electrons, only continuity and energy equations are solved where fluxes are provided by the Sharfetter–Gummel formulation. Transport coefficients are provided as a function of electron temperature by solving Boltzmann's equation. These values are updated every iteration using heavy particle mole fractions, including excited states, averaged over the reactor weighted by the local electron density.

Acceleration techniques are used to speed the rate convergence of computed quantities. During execution of the FKM, the cycle averaged time rate of change in densities is recorded over a period of many rf cycles. The integration is then paused and the densities of species are increased (or decreased) proportional to these average rates and the integration restarted. As different rates of acceleration are applied to different species depending on their derivatives, it is difficult to assign a precise time interval for which the densities are projected into the future. For example, a well con-

Author complimentary copy. Redistribution subject to AIP license or copyright, see http://jap.aip.org/jap/copyright.jsp

verged case will consist of approximately 100–200 iterations through the modules with 0.5–1 μs of actual integration time per iteration (five to ten cycles at 10 MHz) occurring in the FKM (or up to 2000 cycles). For ten cycles of actual time integration, acceleration will typically be applied after two to three cycles of the first six cycles, with no acceleration for the last cycles of the iteration. Based on convergence rates, this is effectively the equivalent of 50–100 times as many cycles. Since different species are accelerated at different rates, it is possible that the net charge density is not conserved through the acceleration process. To prevent unphysical transients in plasma potential, the charge density in each cell is recorded before acceleration. After the acceleration, the electron density is adjusted so that the charge density in each cell is the same as before the acceleration.

The transport of secondary electrons emitted from surfaces is tracked using the EMCS.[12] The electric field as a function of position and phase produced in the FKM is recorded, and these values are interpolated for position and phase during execution of the EMCS. The fluxes and energies of ions striking surfaces are recorded as a function of position which, convolved with the secondary electron emission coefficient, provides the flux of secondary electrons emitted as a function of position along the surface. The secondary electrons are emitted with a Lambertian distribution (essentially a cosine with angle measured respect to the vertical) and an energy of 4 eV. Each pseudoparticle carries a weighting of number of particles per second, or a current. A total of 25 000 electron pseudoparticles are released in the EMCS for each iteration through the HPEM.

The trajectories of the secondary electrons are tracked by integrating their equations of motion while accounting for collisions using Monte Carlo techniques. Each pseudoparticle is tracked until it is collected by a surface, attaches, recombines, or falls below an energy corresponding to the minimum electron excitation threshold, ε_T. If an ionization produces a secondary electron having an energy above ε_T, its trajectory will also be integrated. When removing an electron, its trajectory is checked to make certain it is not at a turn-around point occurring, for example, in a sheath. The electron current striking the surfaces is recorded as a function of position. This current is then used in the FKM to either charge dielectric surfaces (which then appears as displacement current) or to contribute to conduction current if the surface is a metal or has a finite conductivity. The current of electrons falling below ε_T is also recorded as a function of position and used as a source of negative charge in the electron continuity equation in the FKM.

As the pseudoparticle is moved, its energy is recorded on the numerical mesh weighted by the time required to traverse that cell. The resulting electron energy distributions (EEDs) have real units of current/volume. These distributions are convolved with inelastic cross sections to provide source functions for ionization and excitation which are then used in the continuity equations in the FKM.

III. CCP WITH DC AUGMENTATION

dc-CCPs were investigated using only argon to emphasize plasma properties as opposed to plasma chemistry.

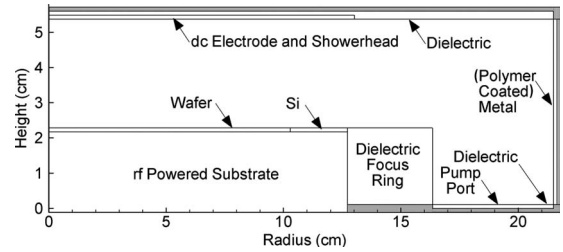

FIG. 1. Schematic of the dc-CCP reactor. The vertical scale is multiplied by 1.5 for clarity.

Plasma and HEE properties in a fluorocarbon containing gas mixture will be discussed in Part II.[11] The reactor used for this study is shown in Fig. 1. (Note that the vertical scale in Fig. 1 is multiplied by 1.5 for clarity.) The substrate, powered at 10 MHz, is 25 cm in diameter and is overlaid with a Si wafer 20 cm in diameter and a Si disk 2.5 cm wide. The substrate is surrounded by a ceramic focus ring ($\varepsilon/\varepsilon_0=8$). The upper electrode to which dc and possibly a second rf bias are applied also serves as a gas shower head. It is 26 cm in diameter and is embedded in a dielectric ($\varepsilon/\varepsilon_0=8$). The dielectric is backed by an electrical ground plane which extends to the side wall. The gap between electrodes is 3.1 cm. An annular pump port surrounds the substrate. Computationally, the pump port passes neutral gas species but is an electrically floating boundary. This was accomplished by having the boundary material for the pump port be a dielectric ($\varepsilon/\varepsilon_0=10$), which passes neutral species.

Powers are separately specified for each applied rf frequency or dc bias. (The rf and dc powers are $P_{\rm rf}$ and $P_{\rm dc}$.) Their voltages are adjusted to deliver those powers. Note that the rf biased substrate generates its own dc bias that is distinct from the applied dc bias on the top electrode. The notations used to describe these voltages are: $V_{\rm rf}$ is the rf voltage applied to the substrate; $V_{\rm rf0}$ is the self-dc bias on the rf electrode; and $V_{\rm dc}$ is the dc bias applied to the upper electrode. In the case of there being two rf frequencies applied, $V_{\rm LF}$ refers to the lower of the rf frequencies applied to the substrate and $V_{\rm HF}$ refers to the higher frequency applied to the showerhead. All rf voltages are expressed as positive amplitudes so that $V_T(t)=V_{\rm rf}\sin(\omega t)+V_{\rm rf0}$ denotes the time dependent voltage on the rf biased substrate. Unless otherwise noted, the secondary electron emission coefficients by ion bombardment γ are 0.15 on the top electrode, wafer, and Si focus ring; 0.05 on the ceramic focus ring; and 0.025 on the top dielectric and sidewall. γ was independent of ion energy.

The base case is Ar, 40 mTorr with a flow rate of 300 sccm (sccm denotes cubic centimeter per minute at STP), $P_{\rm rf}=300$ W, and $P_{\rm dc}=200$ W. To deliver these powers, $V_{\rm rf}=480$ V, $V_{\rm rf0}=-286$ V, and $V_{\rm dc}=-523$ V. Plasma characteristics (electron density n_e; ionization source by bulk electrons S_e; ionization source by beam electrons $S_{\rm eb}$; and source of charge from the beam electrons S_c.) are shown in Fig. 2. The electron density has a maximum value of 3×10^{10} cm^{-3} and is peaked off-axis due to electric field enhancement at the edge of the electrode. The bulk electrons are excluded from both the rf and dc sheaths, approximately

Author complimentary copy. Redistribution subject to AIP license or copyright, see http://jap.aip.org/jap/copyright.jsp

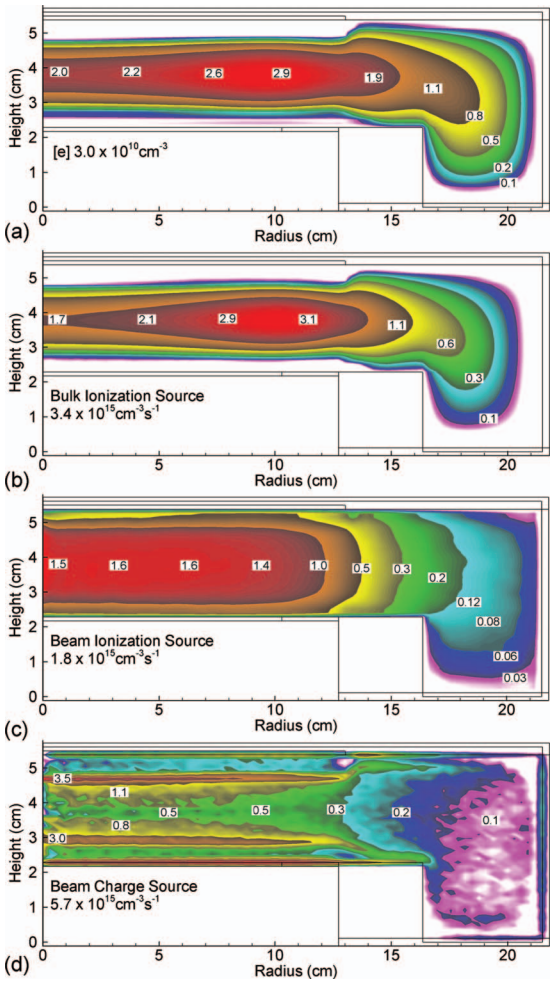

FIG. 2. (Color) Plasma characteristics for the base case (Ar, 40 mTorr, 300 sccm, P_{rf}=300 W and P_{dc}=200 W]. (a) Electron density; (b) ionization source by bulk electrons S_e; (c) ionization source by beam electrons S_{eb}; and (d) source of charge from the beam electrons. Contours span two decades on a logarithmic scale with maximum values shown in each frame. Note the exclusion of bulk electrons from the dc sheath.

0.5-cm-thick at the top dc electrode and 0.27 cm on the lower rf sheath. The sheaths become thinner at larger radii as the maximum plasma density is approached. Due to there being a fairly uniform electron temperature (4.2–4.3 eV), the ionization source by bulk electrons mirrors the electron density, and is maximum at 3.4×10^{15} cm^{-3} s^{-1}. The ionization source by HEE resulting from secondary electron emission from all surfaces has a maximum value of roughly half that of the bulk electrons (1.8×10^{15} cm^{-3} s^{-1}) but provides more than half of the total ionization due to its more uniform distribution. This uniform distribution results from there being secondary electron emission from all surfaces, albeit with varying γ, and there being some pendular motion of secondary electrons trapped between the sheaths.

As discussed by Kawamura *et al.*[5] and Xu *et al.*,[7] secondary electrons emitted from the dc electrode can be reflected by the rf sheath and eventually be trapped in the plasma. As also discussed below, this will occur if $V_{rf}-V_{rf0}>V_{dc}$ assuming the secondary electrons first collisionlessly cross the electrode gap. Trapping likely occurs at lower values of $V_{rf}-V_{rf0}$ given that there is some, on the average, collisional energy loss. In our simulation, trapping occurs when the electron falls below ε_T but outside the sheath to allow for electrons to "turn around" in the sheath. The trapping occurs dominantly near the base of the sheaths, as shown in Fig. 2(d). The charge shown on the surface of the wafer represents those HEEs that are collected by the wafer.

A. HEE distributions

Electrons produced by secondary emission resulting from ion bombardment of the top electrode are accelerated in the adjoining dc sheath. The disposition of those electrons (that is, do they reach the substrate and with what energy) depends on the relative values of the rf and self-dc bias on the substrate and the dc voltage. Ignoring the floating potential and collisions, and assuming sheath thicknesses are small compared to the gap, electrons emitted from the dc electrode will be accelerated into the plasma with an energy ε_s equal to the dc voltage. These electrons are then incident on the opposite rf sheath. If the rf sheath is in its cathodic cycle (that is, $V_T(t)<0$), the HEEs will be decelerated by the rf sheath. If $V_T(t)<V_{dc}$, the HEE will be reflected by the rf sheath back into the plasma. Depending on the phase of the rf voltage, the reflected electron may oscillate between the rf and dc sheaths. The electron will be either eventually collected by the rf electrode or thermalized by collisions and be trapped by the positive plasma potential. In our model, those trapped electrons represent a source of negative charge for the bulk electron distribution or charging of surfaces, as shown in Fig. 2(d).

If a HEE is incident on the rf electrode when $V_T(t)>0$, the rf sheath will accelerate the electron and increase its energy above V_{dc}. The maximum value of the secondary electron energy ε_s is then $\varepsilon_{max}=-V_{dc}+V_{rf}+V_{rf0}$ (where V_{rf0} is typically negative with $|V_{rf0}|<V_{rf}$.). The minimum value of ε_s is then $\varepsilon_{min}=\max(0,-V_{dc}-V_{rf}+V_{rf0})$. For example, the plasma potential for P_{rf}=300 W (V_{rf}=460 V, V_{rf0}=−269 V) and P_{dc}=300 W (V_{dc}=−693 V) during the rf cycle is shown in Fig. 3(a). The EEDs incident on the wafer originating from secondary electron emission from all surfaces for this case are shown in Fig. 3(b). In the absence of collisions (and assuming that the crossing time of electrons is short compared to the rf cycle), the maximum energy of the EED should be 884 eV and the minimum should extend to zero energy. The values obtained from the computed EED agree well with these expectations. Note that the mean free path for inelastic collisions by ionization at the peak energy of the EED, about 900 eV, is nearly 6 cm which is in excess of the gap width. As a result, HEEs nearly ballistically cross the gap on their first crossing.

Note that the plasma potential does not replicate itself on the zero crossings of the rf voltage (lowered by V_{rf0}). The plasma potential is higher during the transition from the anodic to cathodic cycle following the escape of bulk electrons to the substrate. This loss of bulk electrons to the substrate leaves the plasma momentarily more electropositive.

EEDs originating from secondary electron emission incident onto the wafer for $0\le P_{dc}\le 300$ W with P_{rf}=300 W are shown in Fig. 3(b). The biases (V_{rf}, V_{rf0}, and

Author complimentary copy. Redistribution subject to AIP license or copyright, see http://jap.aip.org/jap/copyright.jsp

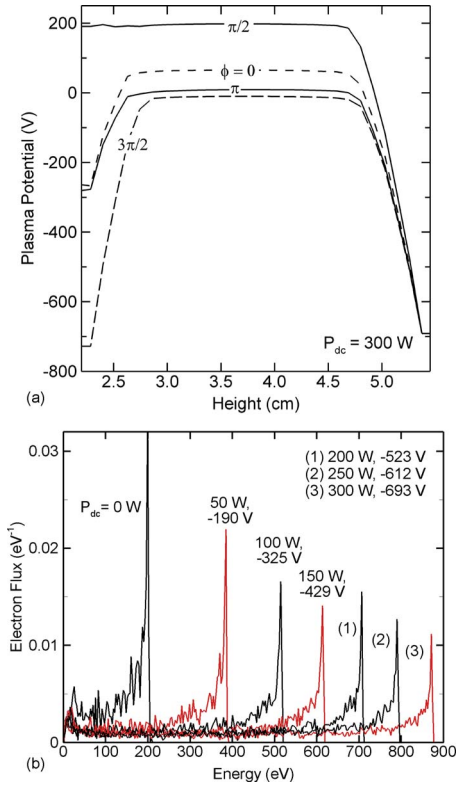

FIG. 3. (Color online) Plasma properties as a function of P_{dc} (Ar, 40 mTorr, 300 sccm, P_{rf}=300 W]. (a) Plasma potential for P_{dc}=300 W at different phases during the rf cycle as a function of height at a radius of 5 cm. The rf electrode is at the left and the dc electrode is at the right. (b) EEDs incident on the wafer originating from secondary electron emission from all surfaces for different P_{rf}. (with the value of V_{dc} noted). Even with P_{dc}=0, HEE fluxes are collected on the wafer.

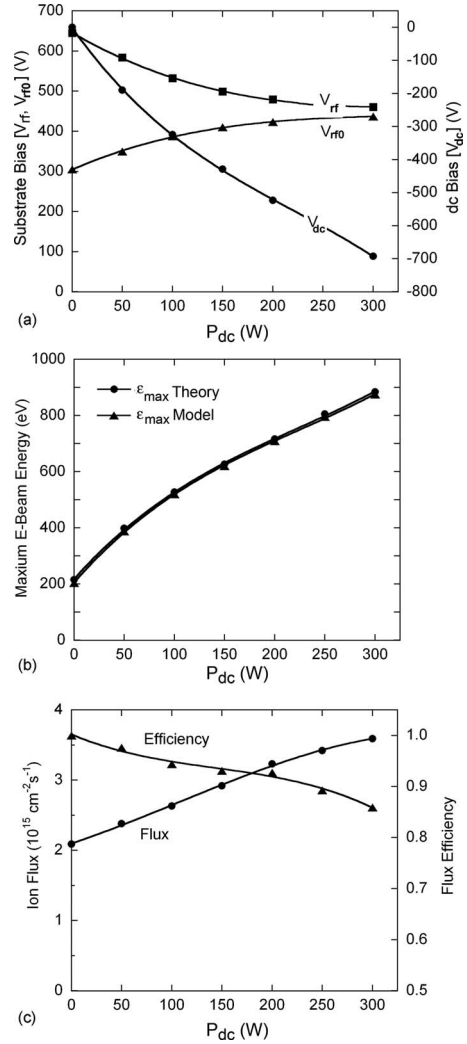

FIG. 4. HEE properties as a function of P_{dc} (Ar, 40 mTorr, 300 sccm, P_{rf} =300 W]. (a) V_{rf}, V_{rf0}, and V_{dc} as a function of P_{dc}; (b) maximum HEE flux energy as a function of P_{dc} (computed and theory); and (c) ion flux and flux efficiency as a function of P_{dc}. The flux efficiency is a measure of the ability of the HEEs to increase the ion flux to the wafer.

V_{dc}) producing these powers, the maximum electron beam energy, ion fluxes, and the ion flux efficiency are shown in Fig. 4. (The ion flux efficiency is the total ion flux per Watt of total power deposition relative to that at P_{dc}=0.) The EEDs generally have a peak at ε_{max} corresponding to the collisionless traversal of secondary electrons through the dc sheath and intersecting the substrate at the peak of the anodic rf cycle. The agreement between the computed values of ε_{max} and those given by our simple scaling law, shown in Fig. 4(b), is within the few electron volts bin size used to compute the EEDs. Since the secondary electrons are emitted essentially randomly through the rf cycle and their crossing times are short compared to the rf cycle, more electrons are collected at the maximum and minimum voltages of the rf cycle. This produces the shoulders to the EEDs at the maximum and minimum energies.

The values of V_{dc} required to deliver P_{dc} decrease sublinearly with P_{dc}. Had the ion flux remained constant while changing P_{dc}, then V_{dc} would have scaled directly with P_{dc}. However, there is an increase in ion flux to the dc electrode when increasing P_{dc} due to the increase in ionization produced by the HEE. Since P_{rf} is being held constant, V_{rf} decreases with increasing P_{dc} as the ion flux to the substrate also increases. This is accompanied by a decrease (less negative) in the self-dc bias, V_{rf0}. As P_{dc} and ε_{max} increase, the cross section for ionization decreases for energies above the maximum in the cross section at 120 eV. As a result, the efficiency of ionization decreases with P_{dc}. Also, due to the reduction in the collision cross section with increasing P_{dc}, a larger fraction of the secondary electrons emitted by the dc electrode are collected by the substrate without having produced significant ionization.

Note that even with P_{dc}=0, there is an energetic electron beam component resulting from secondary electrons. Secondary electrons emitted from the grounded upper electrode will gain an energy of up to $V_{rf}+V_{rf0}$ at the anodic part of the rf cycle. As shown by the plasma potentials in Fig. 5(a), for $V_{rf}+V_{rf0}$=215 V and V_{dc}=0, there is net acceleration of secondary electrons from the top electrode into the rf substrate near the maximum of the anodic portion of the rf cycle. So HEE beams onto the wafer exist to some degree in all rf discharges that have secondary electron emission from the surface opposite the wafer. For a given V_{rf} the energy and magnitude of the flux of the HEEs depends on the self-dc bias V_{rf0}.

To investigate the dependence of the HEE on V_{rf0} with P_{dc}=0, V_{rf} was held constant and V_{rf0} was independently

Author complimentary copy. Redistribution subject to AIP license or copyright, see http://jap.aip.org/jap/copyright.jsp

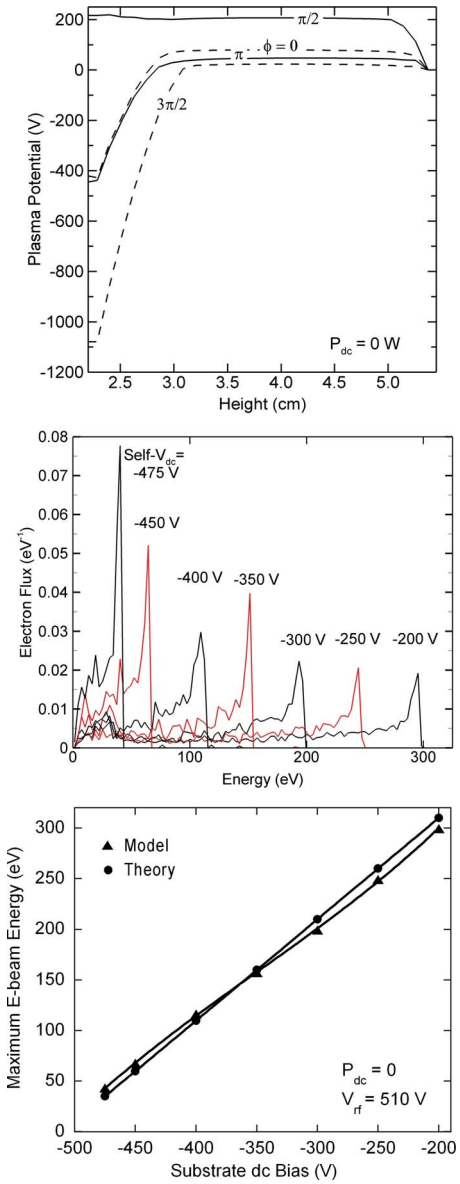

FIG. 5. (Color online) Plasma properties for $P_{dc}=0$ while varying the dc bias on the blocking capacitor on the rf electrode V_{rf0}. V_{rf} is held constant at 510 V. (a) Plasma potential at different phases during the rf cycle for $V_{rf0}=-450$ V. (b) EEDs for the HEE flux onto the wafer as a function of V_{rf0}. (c) Simulated results and theory for the maximum HEE energy as a function of V_{rf0}

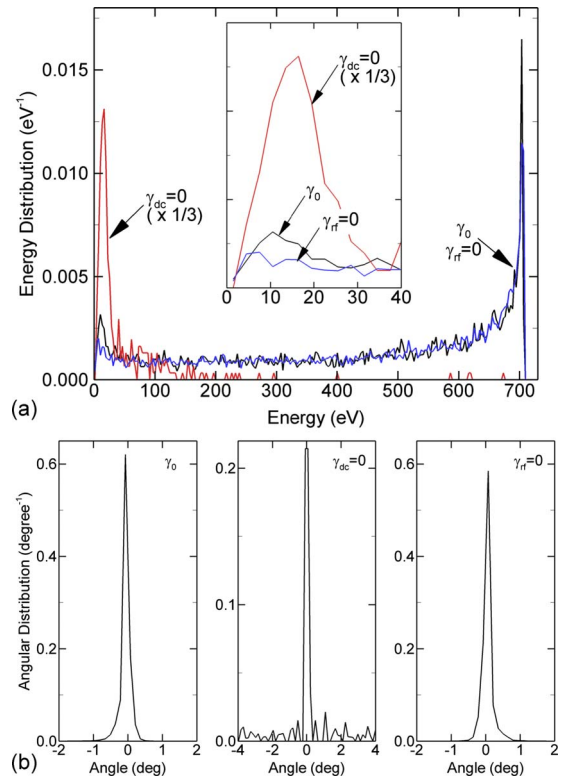

FIG. 6. (Color online) Energy and angular distributions for HEEs incident on the electrode. (a) EEDs at different secondary emission coefficients [γ_0, ($\gamma_{dc}=\gamma_{rf}=0.15$); $\gamma_{dc}=0.15$, $\gamma_{rf}=0$; and $\gamma_{dc}=0$, $\gamma_{rf}=0.15$]. (b) Angular distributions for different γ. The vast majority of the HEE flux about 100 eV results from secondary emission from the dc electrode.

varied. (Note that this does not constitute a self consistent solution but is indicative of the trends.) The EEDs incident onto the wafer resulting from secondary electron emission and the maximum HEE energies are shown in Figs. 5(b) and 5(c) for $V_{rf}=510$ V, $V_{dc}=0$, and $-450 \leq V_{rf0} \leq 0$. The computed maximum energies of the EEDs closely track the theoretical values of $\varepsilon_{max}=V_{rf}+V_{rf0}$. The distribution of electron energies extends to zero energy, which corresponds to the zero crossing in the rf voltage.

To some degree, dc-CCPs operate as hollow cathode discharges. Electrons emitted from one electrode are accelerated by the adjacent sheath and, if not degraded by collisions, are incident on the opposite sheath.[5,7] Depending on the magnitude and phase of the opposite sheath, the incident HEE is either collected or reflected. Assuming that electrons are randomly emitted during the rf cycle from the lower electrode (and ignoring collisions), those electrons emitted when $-(V_{rf}(t)-V_{rf0})<-V_{dc}$ will be reflected by the dc sheath. Then depending on the phase of the rf sheath when they arrive back at the lower electrode, they will again be either reflected by the rf sheath or collected on the substrate. HEE may undergo many crossings across the gap and experience many reflections from sheaths.

To investigate the proportion and distribution of HEE incident onto the wafer that originate from the rf electrode and that have been reflected at least once by the dc sheath, the voltages and dc biases were fixed with $V_{rf}=510$ V, $V_{rf0}=-285$ V, and $V_{dc}=-520$ V (conditions similar to the base case). The secondary emission coefficients for the wafer γ_{rf} and top electrode γ_{dc} were then varied. The results for the normalized energy distribution for the HEE flux to the wafer are shown in Fig. 6(a). The base case (denoted by γ_0) has $\gamma_{rf}=\gamma_{dc}=0.15$, and is compared to cases separately having $\gamma_{rf}=0$ and $\gamma_{dc}=0$. The high energy portion of the electron flux to the substrate is nearly indistinguishable for $\gamma_{rf}=0.15$ and $\gamma_{rf}=0$. This indicates that the vast majority of the HEE flux for these conditions originates from the dc electrode.

When $\gamma_{dc}=0$, the flux dominantly consists of a low energy peak contained below 100 eV. This represents electrons emitted from the substrate during that portion of the rf cycle when the voltage is increasing (becoming more positive). Electrons accelerated by the rf sheath first cross the gap, are reflected by the dc sheath and return to the rf electrode when the sheath voltage is less negative. These electrons are able

Author complimentary copy. Redistribution subject to AIP license or copyright, see http://jap.aip.org/jap/copyright.jsp

to climb the sheath potential to reach the wafer. The energy of the collected HEE is approximately equal to the difference in the rf sheath potential over the time required for the HEE to make two gap crossings. Electrons emitted from the substrate during that portion of the rf cycle when the rf voltage is decreasing (becoming more negative) that cross the gap and are reflected by the dc sheath will also be reflected by the rf sheath. This is because the rf sheath potential is more negative after two gap crossing times than when the electron was originally emitted. The electron is therefore not energetic enough to climb the instantaneous sheath potential. The fluxes to the substrate with $\gamma_{rf}=0$ are diminished by about 1/3 for energies <50 eV compared to $\gamma_{rf}=0.15$. This reduction in flux is due to the absence of electrons emitted from the rf electrode which cross the gap, are reflected by the dc sheath, and collected by the wafer.

Since the ion fluxes to the electrodes change when γ is varied due to the change in the contribution of ionization by HEE, the magnitudes of the HEE fluxes produced by the ion fluxes also change. By normalizing the HEE fluxes by the magnitudes of the ion fluxes that produce them, the relative contributions of electrons to the HEE flux onto the wafer from the rf and dc electrodes can be determined. In doing so, we find that approximately 1/3 of the total HEE flux to the wafer (albeit dominantly below 100 eV) originates from secondary emission from the rf electrode. The remainder (and the vast majority at energies >100 eV) originates from secondary emission from the dc electrode.

The angular distributions of HEEs incident on the wafer are shown in Fig. 6(b). With $\gamma_{rf}=\gamma_{dc}=0.15$ and $\gamma_{rf}=0$, the HEE flux is nearly fully contained within 0.5° of the vertical. Small asymmetries in angle result from two causes. The first is curvature of the dc sheath due to the nonuniform plasma density across the upper electrode. This curvature generates a small off-normal component to the electric field in the sheath which produces a non-normal trajectory. The second cause is electric field enhancement at the edge of the rf electrode that also produces lateral components of the electric field in the sheath. For $\gamma_{dc}=0$, the majority of the HEE flux is also contained within 0.5° of the vertical; however, there is a broad base to the angular distribution due to electrons collected below 30 eV.

B. Collection of dc current

The dc augmentation on the upper electrode produces a time averaged dc current that must be returned to ground. Since the substrate is capacitively coupled it cannot pass a time averaged dc current, and so the current must seek another path to ground. In this particular geometry, the only nondielectric covered surface (or only surface not capacitively coupled) is the metal side wall. (Recall that we prevented dc current from passing through the pump port by covering it with a dielectric). As a result, the dc current must return to ground through the side wall.

For example, the rf cycle averaged magnitude of the current density and current density vectors (showing direction but not magnitude) are shown in Fig. 7 for $P_{dc}=100$ and 300 W. This current density results from the ions and the

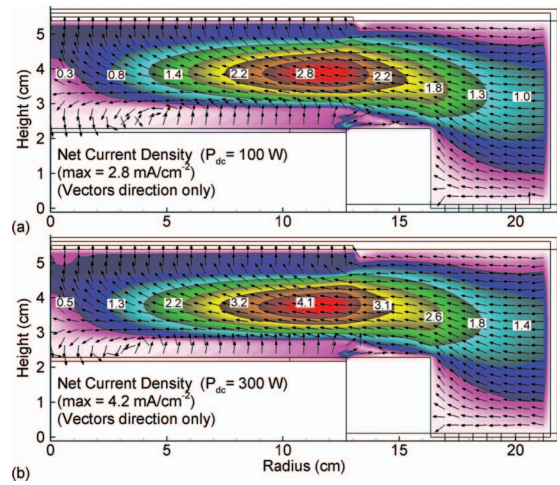

FIG. 7. (Color) The rf cycle averaged magnitude of the bulk electron and ion current densities, and current density vectors for (a) $P_{dc}=100$ W and (b) $P_{dc}=300$ W. The maximum value for each case is noted. The vectors show direction only (not magnitude). A net current flows from the dc electrode to the sidewalls.

bulk electrons, but does not show the contribution of beam electrons which at most would provide approximately γ of the total at the electrode. The dc current density comes out of the side wall, converges through the gap at the edge of the dc electrode as the radius decreases, and is dispersed along the surface of the showerhead. The maximum current density of 2.8 mA/cm^2 for 100 W occurs midgap a few centimeters from the edge of the dc electrode. In order to drive this current, there is a small time averaged electric field from the electrode to the side walls. The dc current density at 300 W closely resembles that of the 100 W case. The peak current density of 4.2 mA/cm^2 is less than twice that of the lower power. The increase in dc power is accomplished by increasing voltage (-325 V for 100 W and -690 V at 300 W) as well as by increasing the current density.

Although the capacitively coupled substrate must, on a cycle averaged basis, pass no dc current, that requirement applies only to the areal integral of the current density. It does not apply locally if there is any significant surface conductivity. In this investigation, we allowed the wafer to have a finite conductivity ($0.01/\Omega$ cm) and so it is able to pass a dc current in the radial direction. The end result is that there is a small dc current that is collected at inner radii on the wafer and returned to the plasma at the outer radii while the areal integral is zero. (Had the substrate been a nonconducting dielectric, the zero-current condition would have been enforced locally as well as globally.) These dc current densities are small (peak values <0.1 mA/cm^2) and are produced by the plasma being nonuniform. In this case, the plasma has a maximum near the edge of the electrode which produces a higher electron beam current by secondary electron emission from the dc electrode. This current is collected on the edge of the wafer and so produces a positive current into the plasma. In this particular case, the recirculating current is largely attributable to the contributions of the HEEs to the wafer. The recirculating current does not occur with $P_{dc}=0$.

Author complimentary copy. Redistribution subject to AIP license or copyright, see http://jap.aip.org/jap/copyright.jsp

Plasma etching is often conducted in polymerizing gas mixtures which deposit polymer films on all surfaces in contact with the plasma. For example, $Ar/C_4F_8/O_2$ gas mixtures are used to etch dielectric materials such as SiO_2.[13] During a few-minute process, many to tens of microns of nominally poorly conducting polymer may be deposited on the inner sidewalls of the reactor. In conventional CCPs, the polymer deposition is not particularly important from the vantage point of the circuit. The polymer layer is thin enough, and its capacitance high enough, that rf current is not significantly impeded by the polymer. (Note that this polymer deposition can change reactive sticking coefficients for radicals and so contribute to the seasoning or drift of reactors. See, for example, Ref. 14.) The deposition of polymer on the sidewalls could be problematic in dc-CCPs as the sidewall may be the location where the dc current returns to ground. The low-conducting nature of the polymer may impede the dc current.

To investigate the consequences of polymer deposition on the sidewalls in dc-CCPs, we added a layer of dielectric to the sidewall with a thickness of 3 mm and conductivity of either $0.1/\Omega$ cm (high conductivity) or $10^{-5}/\Omega$ cm (low conductivity). The dielectric constant of the polymer was adjusted so that its capacitance would be similar to that of a polymer layer of a few hundred microns thickness. This capacitance is high enough to pass the rf current unimpeded. The conditions are otherwise the same as the base case (Ar, 40 mTorr, P_{rf}=300 W, P_{dc}=200 W). The cycle averaged plasma potential as a function of radius at the middle of the gap is shown for the low and high conductivity cases in Fig. 8(a). The high conductivity polymer is able to pass the dc current with a negligible voltage drop. In the low conductivity case, the polymer charges to a negative potential, approximately −20 V, to create a large enough electric field in the polymer to drive the electron current through the polymer into the sidewall. Since the metal sidewall is the reference electrode for the plasma potential, the time averaged plasma potential is decreased by the amount of the voltage drop across the polymer.

The resulting IEADs and EEDs incident onto the wafer are shown in Fig. 8(b) for the high and low conductivity cases. The IEADs are nearly unchanged between the two cases. This is in part because the characteristics of the IEADs are determined by V_{rf}, V_{rf0}, and the rf current, all of which are largely unaffected by the polymer on the sidewall since its capacitance is large enough to pass the rf current. $V_{rf}-V_{rf0}$ increases from 810 to 820 V from the low to high conductivity cases. The maximum energy of the HEE decreases by approximately 20 eV from the low to high conductivity case. There is a small 5 V increase (more negative) in V_{dc} to deliver P_{dc}=200 W, which might increase ε_{max}. However V_{rf0} becomes more negative which then reduces ε_{max}.

To independently investigate the dependence of the HEEs and IEADs on the polymer sidewall coverage, V_{rf} (480 V), V_{rf0} (−285 V), and V_{dc} (−520 V) were held constant as opposed to adjusting them to deliver specified powers. These resulting distributions are shown in Fig. 8(c) for polymer conductivities of 0.1, 10^{-5}, and 10^{-6} Ω^{-1} cm^{-1}. Since V_{rf}, V_{rf0}, and V_{dc} are constant, the HEEs are largely collisionless and the HEEs traverse the gap in a small fraction of the rf period, the EEDs do not significantly change as the polymer conductivity changes. The IEADs incident on the substrate are, however, sensitive to the polymer conductivity. Although the average ion energy is independent of the polymer conductivity since V_{rf} and V_{rf0} are the same, the shape of the IEAD reflects differences in the time dependence of the

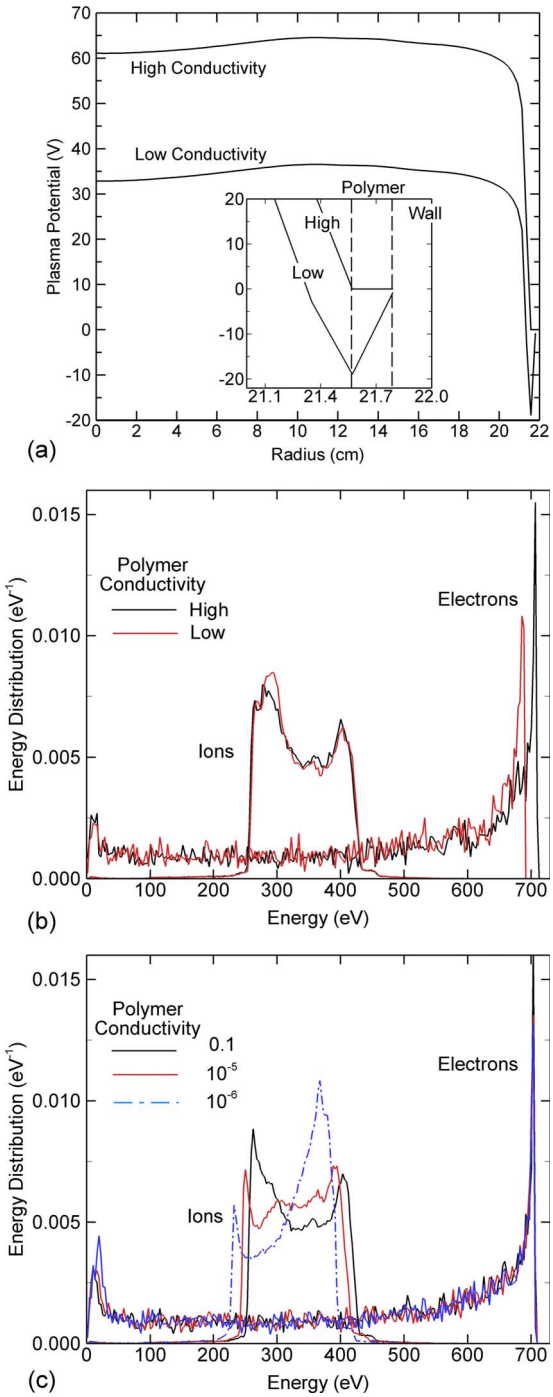

FIG. 8. (Color online) Consequences of polymer deposition on the sidewalls. (a) Cycle averaged plasma potential at the middle of the gap as a function of radius. The polymer on the sidewall has conductivities of 0.1 and 10^{-5} Ω^{-1} cm^{-1}. (b) Energy distributions of ions and HEE to the substrate for low (10^{-5} Ω^{-1} cm^{-1}) and high (0.1 Ω^{-1} cm^{-1}) conductivity polymer. (c) Energy distributions of ions and HEE to the substrate for polymer conductivities of 0.1, 10^{-5}, and 10^{-6} Ω^{-1} cm^{-1} at fixed bias voltages of V_{rf} =480 V, V_{rf0}=−285 V, and V_{dc}=−520 V.

Author complimentary copy. Redistribution subject to AIP license or copyright, see http://jap.aip.org/jap/copyright.jsp

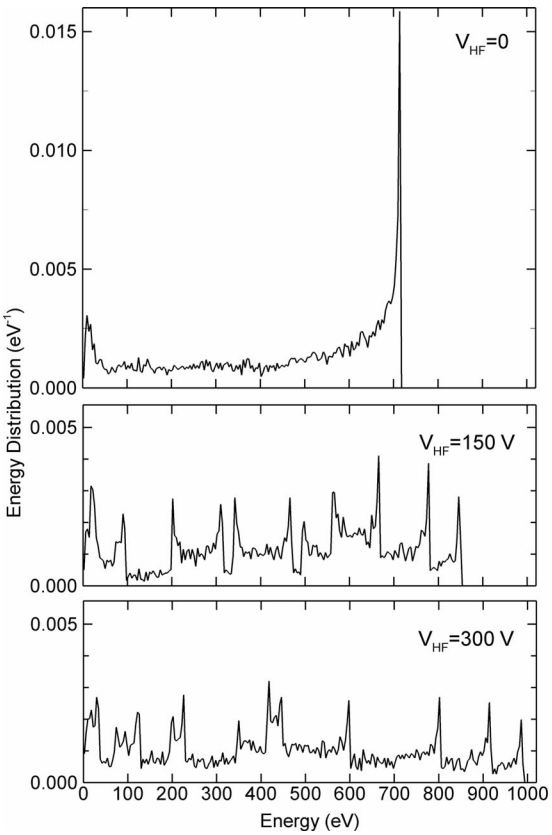

FIG. 9. EEDs for HEE fluxes incident onto the wafer resulting from secondary electron emission for a dual frequency dc-CCP. The values of V_{HF} are (top) 0, (middle) 150 and (bottom) 300 V. The other voltages (V_{LF} =480 V, $V_{rf0,}$=−285 V, V_{dc}=−520 V) were held constant. The HEE flux onto the wafer is modulated by V_{HF} displaced by the change in LF voltage during the time the electron crosses the gap.

plasma potential. With the lower conductivity polymer the plasma potential remains at its maximum value during the cathodic part of the rf cycle for a larger fraction of the cycle, and so the high energy peak of the IEAD is more prominent.

C. Two-frequency CCP

One implementation of the dc-CCP uses two rf frequencies: a low frequency (LF≤10 MHz) on the substrate and a high frequency (HF≥40–100 MHz) on the opposite dc biased electrode. The goal of the two frequency excitation scheme is to separate ion acceleration, more efficiently produced by the LF, from plasma generation, more efficiently produced by the HF. So given that in practice the amplitude of the HF voltage V_{HF}, is less than the magnitude of V_{dc}, the top electrode becomes biased with an rf-modulated dc potential.

To isolate the effects of adding a HF to the dc biased electrode, V_{LF} (480 V) and V_{rf0} (–285 V) on the lower electrode, and V_{dc} (–520 V) on the top electrode were held constant while V_{HF} was varied. The LF is 5 MHz and the HF is 40 MHz for 40 mTorr of argon. The EEDs incident onto the wafer resulting from secondary electron emission for V_{HF} =0, 150 and 300 V, are shown in Fig. 9. With V_{HF}=0, the EED has a maximum energy of 715 eV, which corresponds to $\varepsilon_{max}=-V_{dc}+V_{LF}+V_{rf0}$. The peak of the EED at ε_{max} results from the longer dwell time of the substrate bias at the maximum of the anodic cycle. With V_{HF}=150 and 300 V, the dc bias is modulated on the top electrode with a sinusoidal V_{HF}. The discrete peaks in the EED correspond to a full cycle of modulation of the dc voltage at the HF as the phase of the LF more slowly changes. The maximum energy of the EED should be $\varepsilon_{max}=-V_{dc}+V_{LF}+V_{rf0}+V_{HF}$ or 865 eV for V_{HF} =150 V and 1015 eV for V_{HF}=300 V. The computed values are 853 and 993 eV. The lower computed values result from the finite crossing time across the gap of secondary electrons emitted from the dc electrode. In order to gain an energy ε_{max}, a secondary electron must be emitted at the maximum of the cathodic part of the HF cycle and strike the LF electrode at the maximum of its anodic cycle. In this example, the LF and HF have the same phase and the crossing time across the gap of a 1 keV electron is approximately 2 ns. So during the time between emission of the electron at the HF electrode and it being collected at the LF electrode, the substrate voltage will have decreased by about 24 V, which accounts for the difference between the theoretical and computed values. The HEE distribution onto the substrate can therefore be tuned to some degree by the phase differences and frequencies of the LF and HF potentials.

D. Low frequency

In many applications of HAR etching, particularly in dual frequency CCPs, the substrate bias is at frequencies as low as 1–2 MHz. To investigate the consequences of the frequency of the substrate bias on the EEDs incident on the wafer resulting from secondary electron emission, the substrate bias was varied between 2 and 16 MHz. Again, to isolate the effects of changing only the frequency of the substrate bias, V_{rf} (480 V) and V_{rf0} (–285 V) on the lower electrode and V_{dc} (–520 V) on the top electrode were held constant. The resulting EEDs are shown in Fig. 10. On the scale of the entire range of energies, the EEDs for frequencies of 2–16 MHz are nearly indistinguishable. The high energy peak of the EED and the maximum electron energy do, however, systematically vary. The peak and maximum energy decrease with increasing frequency. For a bias of 2 MHz, the maximum energy is 712 eV, which is nearly the same as the maximum theoretical energy of $\varepsilon_{max}=-V_{dc}+V_{rf}+V_{rf0}$ or 715 eV. The maximum energy decreases to 702 eV at 16 MHz. This is in large part a transit time effect. In order for a secondary electron to gain the maximum energy, it must be emitted from the dc biased electrode at the peak of the anodic cycle and cross the electrode gap before the substrate bias appreciably changes. The time required for a 700 eV electron to cross the electrode gap is about 1.8 ns. During this time, the voltage on the substrate near the peak of the anodic cycle at 16 MHz will have changed by 10 eV. Electrons emitted from the dc electrode on the ascending portion of the anodic cycle (bias becoming more positive) will gain energy larger than that corresponding to the phase of their emission because the substrate sheath potential is increasing during its transit time. Electrons emitted at the peak and descending portion of the rf cycle (bias becoming more negative) will gain less energy, in this case about 10 eV at 16 MHz.

Author complimentary copy. Redistribution subject to AIP license or copyright, see http://jap.aip.org/jap/copyright.jsp

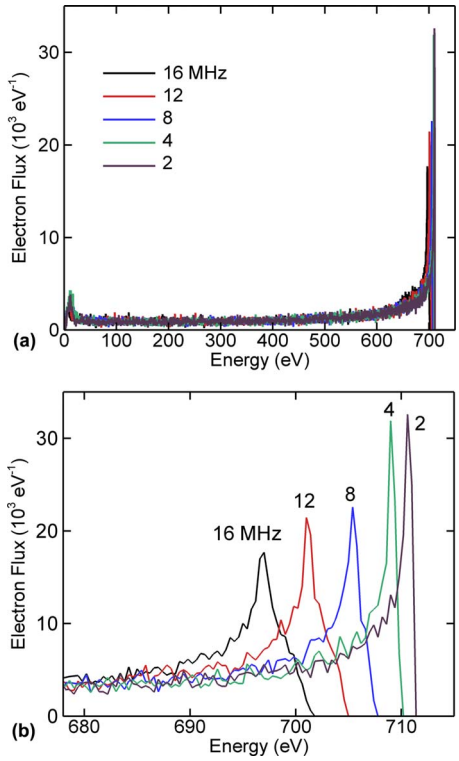

FIG. 10. (Color online) EEDs for HEE fluxes incident onto the wafer resulting from secondary electron emission while varying the frequency of the bias on the lower electrode. (a) Full energy range and (b) expansion of scale at high energy. The voltages (V_{rf}=480 V, V_{rf0}=−285 V, and V_{dc}=−520 V) were held constant. The HEE flux onto the wafer is not significantly changed by the bias frequency though the maximum energy decreases by a few electron volts at high energy due to the finite cross time of secondary electrons.

IV. CONCLUDING REMARKS

Characteristics of HEE fluxes to the substrate were computationally investigated in single and dual frequency dc-CCPs. Electrons emitted from either the rf or dc electrodes are accelerated by the adjacent sheath and, if not degraded by collisions, are incident on the opposite sheath. Depending on the magnitude and phase of the rf sheath, the incident HEE from the dc electrode is either collected or reflected. HEEs from the dc electrode are collected with energies $\max(0, -V_{dc}-V_{rf}+V_{rf0}) < \varepsilon_{s,} <= -V_{dc}+V_{rf}+V_{rf0}$. Even with $V_{dc}=0$, HEE fluxes as large as $V_{rf}+V_{rf0}$ can be collected by the wafer. Approximately 30% of the HEE flux collected by the wafer, mostly at energies <100 eV, can be attributed to secondary electrons emitted by the rf biased substrate and reflected by the dc sheath. The current emitted by the dc electrode must return to ground through a noncapacitively coupled surface. In our model, that surface is the grounded sidewall. When the sidewall is coated with a poorly conducting polymer, charge will build up to push the dc current through the coating. This could result in sparking under extreme conditions. When applying a HF bias to the dc electrode in a dual frequency CCP, the HEE flux is modulated by the HF voltage. The precise energy spectrum of the HEE flux collected by the substrate then depends on the relative phases of the LF and HF biases. The HEE distribution onto the substrate can therefore be tuned to some degree by the phase differences and frequencies of the LF and HF potentials. The consequences of HEE fluxes on etching of high-aspect-ratio SiO_2 features using fluorocarbon plasmas are discussed in our companion paper.[11]

ACKNOWLEDGMENTS

This work was supported by Tokyo Electron Ltd., the Semiconductor Research Corp., and Micron Corp.

[1]S.-B. Wang and A. E. Wendt, J. Appl. Phys. **88**, 643 (2000).
[2]T. Novikova, B. Kalache, P. Bulkin, K. Hassouni, W. Morscheidt, and P. Roca i Cabarrocas, J. Appl. Phys. **93**, 3198 (2003).
[3]T. Kitajima, Y. Takeo, Z. Lj. Petrovic, and T. Makabe, Appl. Phys. Lett. **77**, 489 (2000).
[4]E. Kawamura, M. A. Lieberman, A. J. Lichtenberg, and E. A. Hudson, J. Vac. Sci. Technol. A **25**, 1456 (2007).
[5]E. Kawamura, A. J. Lichtenberg, and M. A. Lieberman, Plasma Sources Sci. Technol. **17**, 045002 (2008).
[6]K. Denpoh and P. L. G. Ventzek, J. Vac. Sci. Technol. A **26**, 1415 (2008).
[7]L. Xu, L. Chen, M. Funk, A. Ranjan, M. Hummel, R. Bravenec, R. Sundararajan, D. J. Economou, and V. M. Donnelly, Appl. Phys. Lett. **93**, 261502 (2008).
[8]S. Welch, K. Keswick, P. Stout, J. Kim, W. Lee, C. Ying, K. Doan, H. S. Kim, and B. Pu, Semicond. Int. **32**, 18 (2009).
[9]M. Kiehlbauch, "Reverse masking profile improvements in high aspect ratio etch," U.S. Patent Application No. 2009/7553770 (2009).
[10]J. Bing, E. A. Edelberg, and T. Yanagawa, "Reducing twisting in ultra-high aspect ratio dielectric etch," U.S. Patent Application No. 2008/0119055 (2008).
[11]M. Wang and M. J. Kushner, J. Appl. Phys. **107**, 023309 (2010).
[12]M. J. Kushner, J. Phys. D **94**, 194013 (2009).
[13]X. Li, L. Ling, X. Hua, M. Fukasawa, G. S. Oehrlein, M. Barela, and H. M. Anderson, J. Vac. Sci. Technol. A **21**, 284 (2003).
[14]B. Zhou, E. A. Joseph, S. P. Sant, Y. Liu, A. Radhakrishnan, L. J. Overzet, and M. J. Goeckner, J. Vac. Sci. Technol. A **23**, 1657 (2005).

Author complimentary copy. Redistribution subject to AIP license or copyright, see http://jap.aip.org/jap/copyright.jsp